Korean J. Chem. Eng., 34(5), 1444-1455 (2017)
DOI: 10.1007/s11814-017-0031-3

pISSN: 0256-1115
eISSN: 1975-7220

Flux, antifouling and separation characteristics enhancement of nanocomposite polyethersulfone mixed-matrix membrane by embedding synthesized hydrophilic adipate ferroxane nanoparticles

Masoud Rahimi*, Soheil Dadari*,†, Sirus Zeinaddini, and Elham Mohamadian*****

*CFD Research Centre, Department of Chemical Engineering, Faculty of Engineering, Razi University, Kermanshah, Iran
**Water and Wastewater Research Center (WWRC), Department of Applied Chemistry, Faculty of Chemistry, Razi University, Kermanshah, Iran
***Department of Biology, Faculty of Science, Razi University, Kermanshah, Iran
(*Received 2 December 2016 • accepted 6 February 2017*)

Abstract−Polyethersulfone (PES) nanofiltration (NF) membranes were prepared by blending of synthesized hydrophilic adipate ferroxane nanoparticles (AFNPs) as a novel multifunctional nanofiller via the phase inversion method. The water contact angle measurement indicated the higher hydrophilicity of the NF membranes. The water flux of the membranes improved significantly after the addition of AFNPs, from 10.4 to 32.2 kg/m^{2}h. Antifouling characteristics of AFNPs/PES membranes were improved by increased hydrophilicity and decreased membrane surface roughness. The 0.6 wt% AFNPs/PES membrane exhibited the highest FRR (96%) and the lowest irreversible fouling resistance (6%). The nanofiltration performance of the prepared membranes was evaluated by dye removal and salt retention. The results proved the high dye removal capability of modified membranes (98% rejection) compared with the unfilled PES membrane (89% rejection). The salt retention sequence for membrane with 0.2 wt% of nanoparticles was Na_2SO_4 (70%)>$MgSO_4$ (60%)>NaCl (18%).

Keywords: Nanofiltration, Nanocomposite, Synthesized Adipate Ferroxane Nanoparticles, Separation Performance, Antifouling Ability

INTRODUCTION

Nanofiltration (NF) as a pressure driven membrane processes has been used extensively, especially in water and wastewater treatments. To date, many polymeric materials such as cellulose acetate, polyamide, polyimide, polysulfone and polyethersulfone have been used for NF preparation [1]. Among these, polyethersulfone is selected for different purposes in membrane preparation because of its good thermal, mechanical, biological, and chemical stability [1]. Despite these advantages, membrane fouling is an obstacle for wide application of PES and has hindered membrane processes. Dramatic decreases in permeation flux due to fouling lead to substantial increases in energy demand, shorter membrane lifetime, regular membrane cleaning, unpredictable separation performance, and increased operational and maintenance costs [2,3]. Therefore, fouling is a severe problem for membrane separation processes which must be prevented or mitigated to reduce its negative impacts.

Generally, the pretreatment of fluid before the membrane unit, appropriate membrane selection, adjustment of operating design, and cleaning process after long-time filtration are identified as strategies to control fouling to some extent [4-9].

Many studies have reported that membrane hydrophilicity and morphology as the heart of the membrane process must be modified to produce membranes that are significantly improved in reducing the propensity for fouling [10]. For this purpose, several approaches such as coating with hydrophilic polymer [11,12], grafting [13,14], embedding hydrophilic nanoparticles (NPs) [15,16] or hydrophilic polymers and monomers [17,18] have been suggested.

Among the various modification techniques, the method of embedding nanoparticles into a polymer matrix, namely mixed-matrix membrane (MMM), has demonstrated outstanding separation properties and has been the subject of worldwide academic studies because of significant changes in the membrane's mechanical, thermal, magnetic, morphology, and hydrophilicity properties and especially the alleviation of membrane fouling compared with non-incorporated membranes [19-22].

Many inorganic nanofillers such as TiO_2 [23], Al_2O_3 [24], SiO_2 [25], boehmite [15], graphene oxide [26], carbon nanotubes [27], and Fe_3O_4 [28] have been used in polymeric membranes to improve permeation flux and fouling mitigation.

Iron oxide nanomaterials (NMs) have been widely studied from the scope of synthesis and utilization because of their size in nanorange, high surface area-to-volume ratios, and super-paramagnetism with novel properties and functions [29]. The high reactivity of iron as pure metal nanoparticles promotes its use as an iron compound instead of a pure one for incorporation into polymeric membranes [28,30,31]. Moreover, despite the intrinsic properties of metal oxide nanoparticles, fabrication of nanocomposite membranes using these materials faces some problems such as agglom-

†To whom correspondence should be addressed.
E-mail: soheildadari@gmail.com, soheildadari@yahoo.com

eration and weak interaction of the interface between the nanoparticles and the polymer matrix. Therefore, to overcome these problems, modification with desired functional groups can be applied to obtain nanoparticles with new properties and capabilities [32].

Daraei et al. made a blend of PES with PANI/Fe_3O_4 to obtain increased hydrophilicity and Cu (II) removal. They reported that, although the Cu (II) removal was increased, the permeation flux of embedded membranes decreased as a result of pore blockage by accumulated nanoparticles [33]. Ghaemi et al. solved this problem by embedding four functionalized Fe_3O_4 nanoparticles in a polyethersulfone matrix and found that hydrophilic groups preferentially concentrate at the membrane surface [32].

Ferroxane nanoparticles are a subcategory of functionalized iron oxides that are prepared through a reaction of iron oxy-hydroxides and carboxylic acids. These nanoparticles have been employed in effluent removal [34-36]. Zhang et al. studied the effects of ferroxane and goethite nanoparticles in a proton exchange membrane for fuel cell application. Their results showed the higher proton conductivity of ferroxane than goethite [37]. Cortalezzi et al. made an ultrafiltration ceramic membrane with ferroxane nanoparticles and investigated the size of the nanoparticles and the kinetics of the reaction on membrane performance [38].

In this study, the polyethersulfone (PES) nanofiltration membranes were prepared by blending of synthesized hydrophilic adipate ferroxane nanoparticles (AFNPs). The main aim of this research was to simultaneously increase the permeate flux, nanofiltration efficiencies, and antifouling properties enhancement. The effects of carboxylated nanoparticles in the casting solution on membrane characteristics, such as hydrophilicity, permeation flux, morphology, antifouling properties, and nanofiltration performance, were examined. The membrane structure and surface properties were analyzed using overall porosity, water contact angle, atomic force microscopy (AFM), and scanning electron microscopy (SEM) measurements.

Fouling resistance and the flux recovery ratios of plain and modified mixed-matrix membranes were studied using milk powder filtration. The salt retention and dye removal capabilities were also performed by rejection of Na_2SO_4, $MgSO_4$, NaCl solutions and direct red 16 dye.

METHODS

1. Materials

All chemicals employed in experiments were of reagent grade. Polyethersulfone (Ultrason E 6020P, M_w=58,000 g/mol and glass transition temperature T_g=225 °C) and dimethylacetamide (DMAc) as solvent were provided by BASF Co., Germany. Polyvinylpyrrolidone (PVP) with a 25,000 g/mol molecular weight was purchased from Mowiol, Germany. KOH, adipic acid, and iron nitrate were obtained from Merck to synthesize adipate ferroxane nanoparticles. The direct red 16, $C_{26}H_{17}N_5Na_2O_8S_2$ (M_W=637.26), with a purity of 99% was purchased from Alvan Sabet Company, Iran. Distilled water was used throughout this study.

2. Synthesis of Adipate Ferroxane Nanoparticles

The adipate ferroxane was synthesized in two stages [39]. In the first stage, goethite nanoparticles with multiple OH functional groups were prepared and in the second stage, functional groups of goethite were reacted with adipic acid to synthesis adipate ferroxane nanopar-

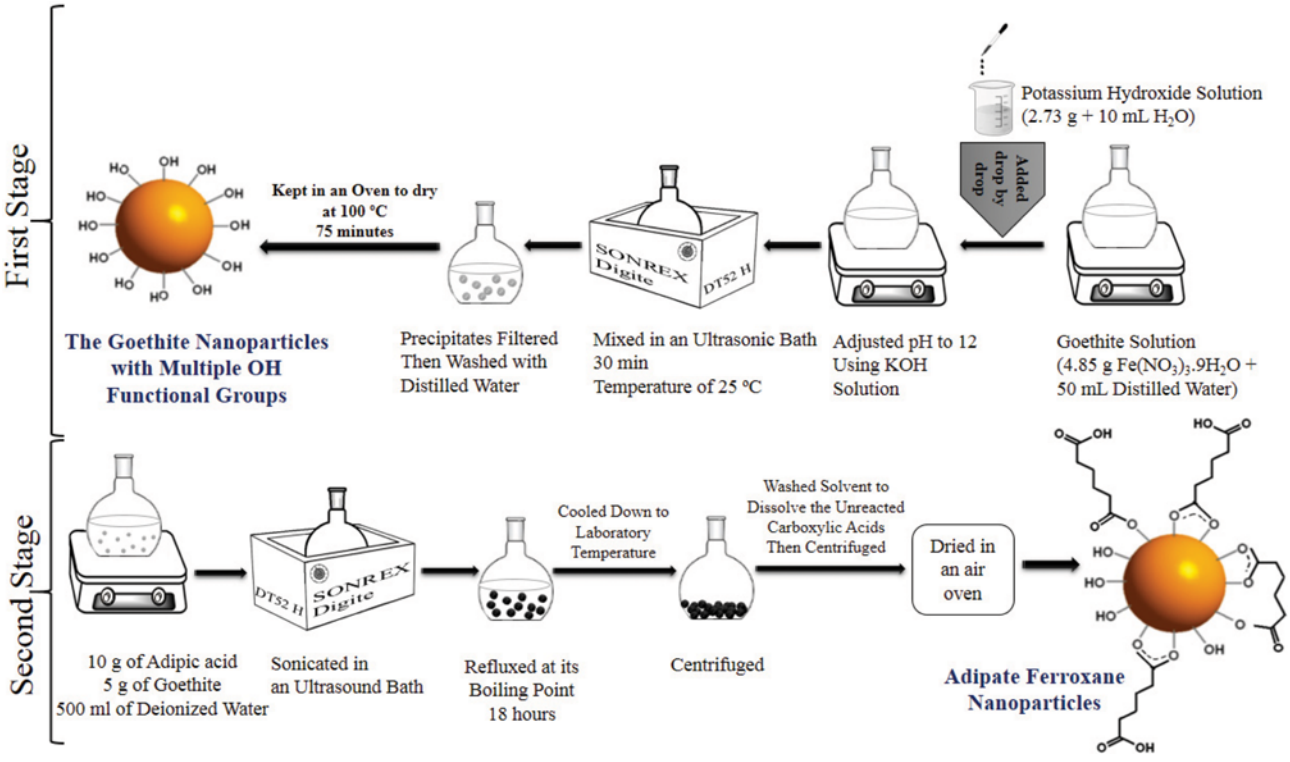

Fig. 1. The schematic diagram for synthesis goethite and adipate ferroxane.

Table 1. The compositions of casting solutions

Membrane code	PES (wt%)	PVP (wt%)	AFNPs (wt%)
M_0	20.0	1.0	-
M_1	20.0	1.0	0.2
M_2	20.0	1.0	0.6
M_3	20.0	1.0	1.0

ticles. Fig. 1 shows the schematic diagram for synthesis of goethite and adipate ferroxane nanoparticles.

3. Fabrication of PES Nano-enhanced Membranes

Asymmetric adipate ferroxane nanoparticles-embedded PES nanofiltration membranes were prepared via phase inversion induced by immersion precipitation using casting solutions containing PES (20 wt%), PVP (1 wt%), and the proper amount of nanoparticles in DMAc as solvent. Compositions of all casting solutions are presented in Table 1.

Briefly, precise percentages of nanoparticles (0.2, 0.6 and 1.0 wt%) were added into DMAc and dispersed by sonication for 30 min to improve homogeneity using DT 102H Bandelin Ultrasonic (Germany). Then, PES and PVP were dissolved into the dope solution by continuous stirring at 400 rpm for 24 hours to reach a homogeneous solution of polymer. Bubbles were removed by sonication wave for 10 min and then casted on a glass plate using a homemade film applicator with 200 μm thickness. The glass plate was subsequently immersed in a coagulation bath of deionized water without any evaporation. The formed membranes were stored in fresh distilled water for 24 hours to remove residual solvent and pore-forming agent. Finally, two filter papers were used to sandwich the prepared membranes for 24 hours at room temperature.

4. Characterization of the Nanocomposite Mixed-matrix Membranes

Fourier transform infrared (FT-IR) spectra of nanoparticles were recorded in the range of 300-4,500 cm^{-1} using a Bruker spectrometer (TENSOR 27). Philips-XL30 and Cambridge scanning electron microscopes (SEM, CamScan MV2300) were used to observe a cross-section of the prepared membranes. The pre-membranes were fractured by freezing in liquid nitrogen. Then, they were sputtered with gold and produced electric conductivity. They were observed by microscope at 17 kV.

Atomic force microscopy was applied to evaluate the roughness and surface morphology of the prepared membranes. Nanosur® Mobile S scanning probe-optical microscope (Switzerland) provided with Nanosur® MobileS software (version 1.8) was used. Membrane samples (approximately 1 cm^2) were fixed onto a specimen holder and scanned by tapping mode in air.

The hydrophobicity of the membrane was quantified by measuring water drop contact angle with a goniometer (G10, KRUSS, Germany). Contact angle was estimated in captive bubble mode. There was no damage to the structure of the pores because of drying. All contact angle measurements were taken using 2 μl of deionized water. To minimize experimental errors, contact angles were measured at five random locations for each sample and the average was reported.

UV-vis spectrophotometer (DR5000, Hach, Jenway, USA) was used to analyze the concentration of the direct red 16 by measuring the absorbance at λ max=526 nm using an appropriate calibration curve [40].

The gravimetric method was used to determine overall porosity (ε) using the following equation [41]:

$$\varepsilon = \frac{\omega_1 - \omega_2}{A \times l \times d_w} \quad (1)$$

where ω_1 is the weight of the wet membrane (kg); ω_2 is the weight of the dry membrane (kg); l is the membrane thickness (m); d_w is water density (998 kg/m^3), and A is the membrane surface (m^2). The membrane thickness was measured using a digital micrometer (Mitotoyo, Japan).

5. Permeation Test

To characterize the fabricated membrane, the pure water flux, dye rejection, and milk powder fouling tests were measured in a batch type, dead-end cell (150 ml volume) with a membrane surface area of 12.56 cm^2; the cell was fitted with a pressure gauge (see Fig. 2). Pressurized nitrogen gas was used to force the liquid through the membrane.

Each membrane was initially pressurized at 6 bar for 60 min; then the transmembrane pressure was reduced to 4 bar of operating pressure. Pure water flux $j_{w,1}$ (kg/m^2 h) was estimated using the following equation:

$$j_{w,1} = \frac{Q}{A\Delta t} \quad (2)$$

where Q (kg) is weight of permeated water, A (m^2) is membrane area, and Δt (h) is permeation time.

To evaluate nanofiltration performance and the dye removal capabilities of the fabricated membranes, the retention of direct red 16 was studied. The concentration of prepared aqueous feed dye solution was 30 mg/L, comparable to the textile wastewater concentration [41]. Rejection (R) during the experiment is defined as follows [42]:

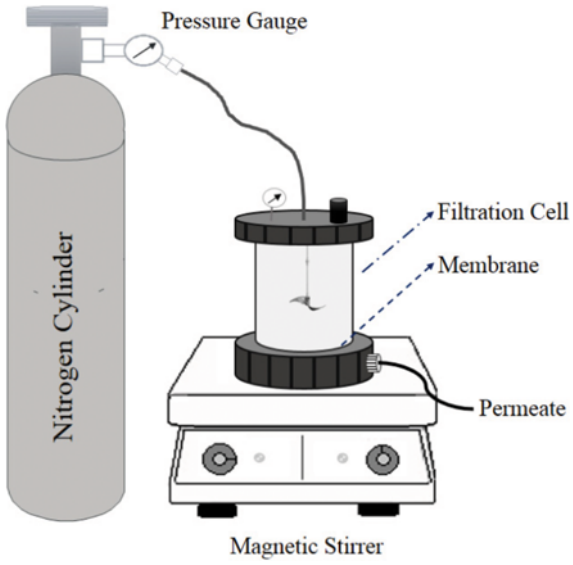

Fig. 2. Schematic diagram of dead-end system.

$$R\,(\%) = \left(1 - \frac{C_p}{C_f}\right) \times 100 \quad (3)$$

where C_p and C_f are particular concentrations in permeate and feed, respectively.

6. Analysis of Membrane Fouling

After the water flux tests, the milk powder solution with a concentration of 8,000 mg/L (as the fouling agent) was immediately replaced in the stirred cell. Then its flux, Jp (kg/m^2 h), was calculated through the membranes based on the water quantity permeated at 4 bar for 60 min.

The sealed membranes were washed with distilled water for 15 min. Afterwards, the water flux of the cleaned membranes, $J_{w,2}$ (kg/m^2 h), was estimated once more. The flux recovery ratio (FRR) was defined as follows [16]:

$$FRR(\%) = \left(\frac{j_{w,2}}{j_{w,1}}\right) \times 100 \quad (4)$$

Generally, a higher FRR indicates better antifouling properties of the nanofiltration membrane.

The reversible fouling ratio (R_r), irreversible fouling ratio (R_{ir}) and total fouling (R_t) were measured using the following equations to analyze the fouling process in detail [27]:

$$R_r\,(\%) = \left(\frac{j_{w,2} - j_p}{j_{w,1}}\right) \times 100 \quad (5)$$

$$R_{ir}\,(\%) = \left(\frac{j_{w,1} - j_{w,2}}{j_{w,1}}\right) \times 100 \quad (6)$$

$$R_t\,(\%) = \left(1 - \frac{j_p}{j_{w,1}}\right) \times 100 \quad (7)$$

RESULTS AND DISCUSSION

1. Characterization of Adipate Ferroxane Nanoparticles

The representative spectrum acquired by FTIR is shown in Fig. 3. Analysis of peaks of FTIR spectrum reveals details about the molecular structure of the samples. There are two absorption peaks at 1,400 cm^{-1} and 1,525 cm^{-1} corresponding to the carboxylates symmetric and asymmetric stretching mode. It binds the molecules of adipic acid with the surface of goethite nanoparticles. A well pronounced peak of carbonyl groups of the carboxylics is visible at 1,687 cm^{-1} arising from the free adipic acid molecules which have not reacted. A broad band is apparent in the 2,400-3,400 cm^{-1} region for OH vibrations of free carboxylated groups.

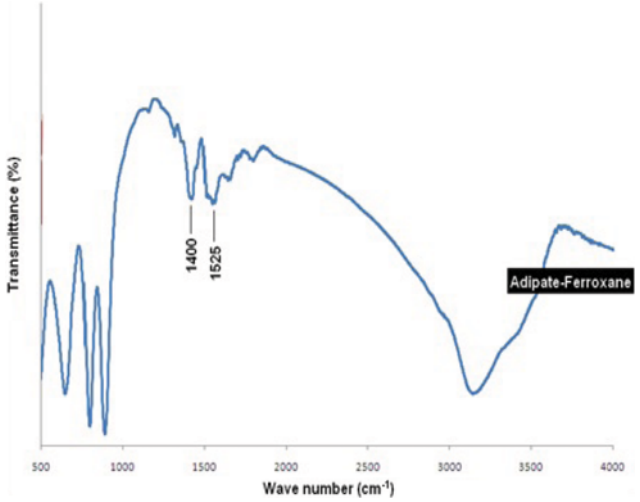

Fig. 3. FTIR spectra of adipate ferroxane.

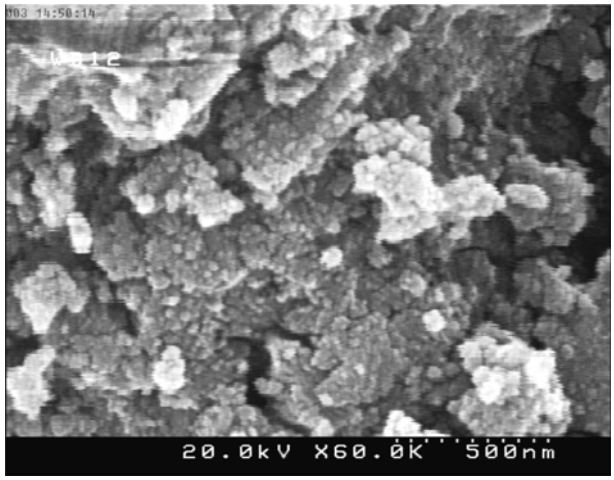

Fig. 4. SEM image of adipate ferroxane nanoparticles.

To further characterize the prepared nanoparticles, SEM analyses were performed, and the results are shown in Fig. 4. The adipate ferroxane nanoparticles are spherical with average diameters of about 40-70 nm.

2. Pure Water Flux

The pure water flux of bare and modified membranes is depicted in Fig. 5. The results clearly show that adding nanoparticles to the polymer matrix led to an increase in pure water permeation through the membranes compared with the bare PES membrane.

The permeation flux of the membranes can be affected by many factors involving surface pore size, cross-section morphology, skin layer thickness, dope solution viscosity, and hydrophilicity [16]. The cross-sectional SEM photographs of the prepared membranes with different concentrations of the AFNPs with two magnifications are presented in Fig. 6.

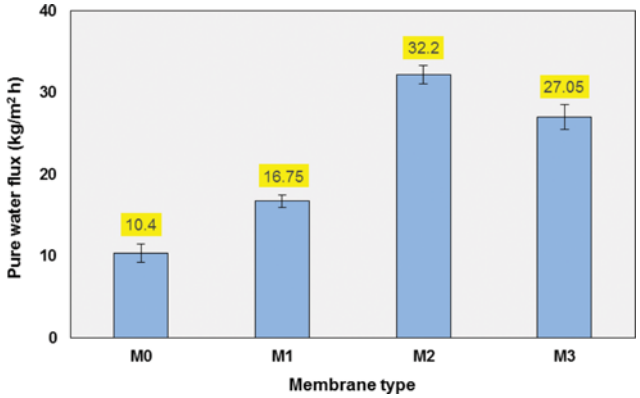

Fig. 5. Pure water flux of the membranes at 4 bar.

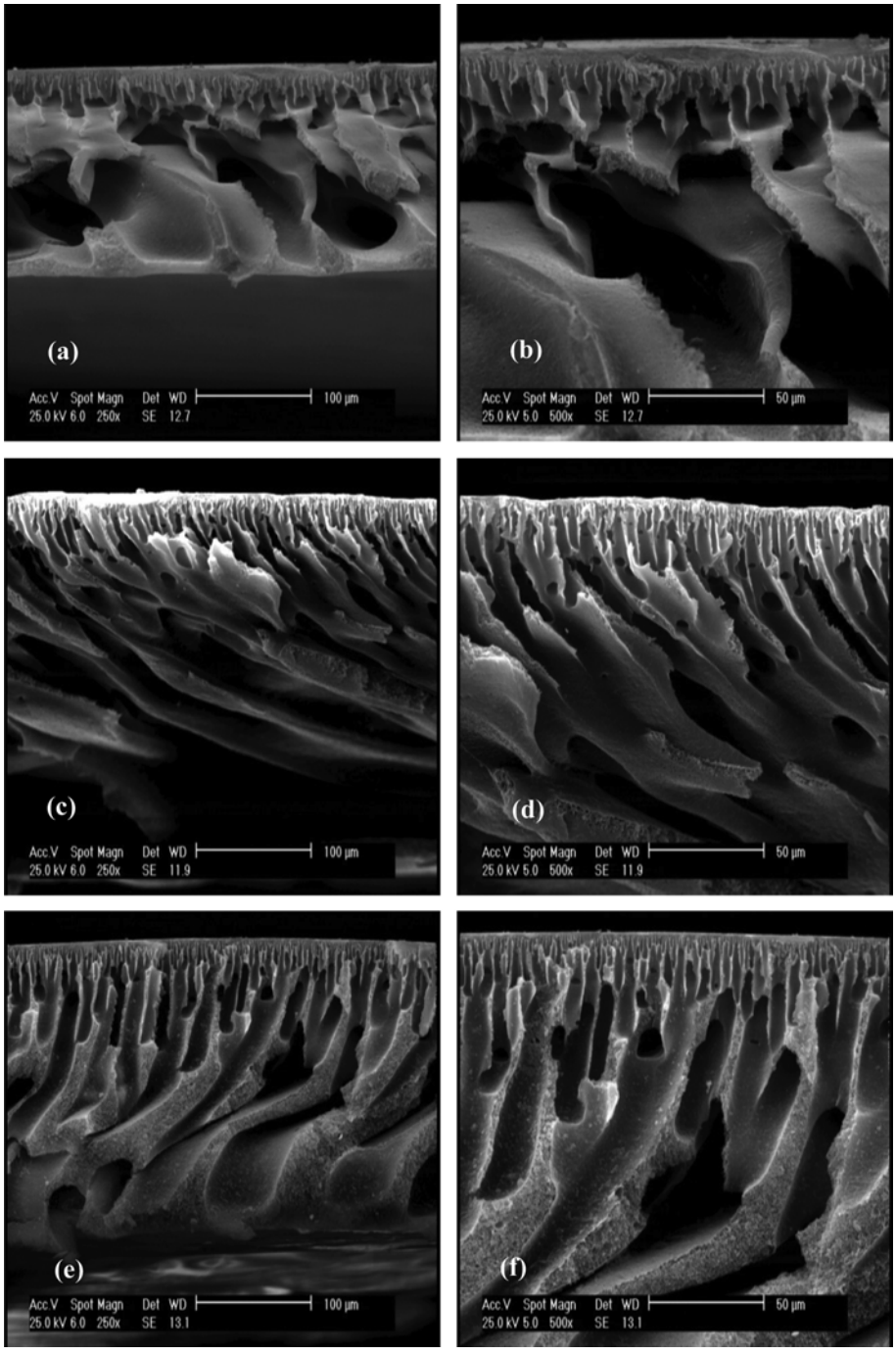

Fig. 6. Cross-sectional SEM images of the prepared membranes: (a) and (b) Unfilled PES, (c) and (d) 0.2 wt%, (e) and (f) 0.6 wt%, (g) and (h) 1 wt%.

As shown in Fig. 6, all the membranes had typical asymmetric porous structures with a dense skin top-layer followed by a finger-like porous sub-layer. The bare PES membrane consisted of a dense skin top-layer with (very) low porosity as well as a non-uniform thickness of sub-layer. The figures of embedded membranes clearly indicate that addition of adipate ferroxane NPs into casting solution decreases the thickness of skin top-layer and increases the uniformed porosity of both top and sub-layer of blended membranes in comparison with unmodified PES membrane this trend can be seen in similar studies [42,43]. The higher magnification SEM images clearly show these changes. The thickness of skin top-layer decreased when the concentration of adipate ferroxane nanoparticles increased from 0.2 wt% to 0.6 wt%. From the Fig. 6(g) and (h), high concentration of adipate ferroxane nanoparticles (1.0 wt%) in the casting solution caused the denser skin top-layer with the lower porosity, because of increasing of the viscosity of the casting solution by addition high concentration of adipate ferroxane NPs (more than 0.6 wt%) which made a delay in the ex-

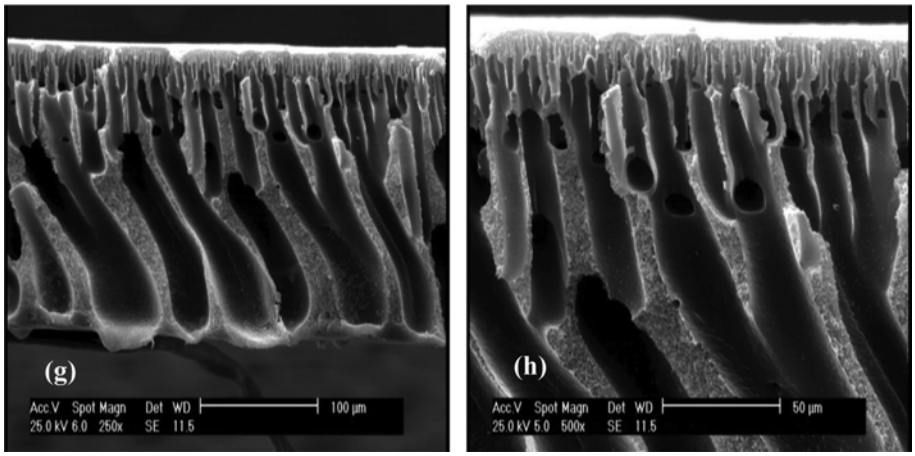

Fig. 6. Continued.

Table 2. The contact angle and porosity of prepared membranes

Membrane type	M_0	M_1	M_2	M_3
Contact angle (°)	68.12	60.33	55.04	54.73
Porosity (%)	73.8±3.7	81.5±2.9	87.1±4.1	82.1±4.3

change rate between solvent and nonsolvent during the phase inversion. Furthermore, the effects of addition of AFNPs in casting solution on membrane structure and pure water flux are discussed in the following sections.

Adding adipate ferroxane to the casting solution resulted in a growth in membrane skin top-layer and sub-layer porosity. To prove the increment of membrane porosity, the overall porosity information of synthesized membranes is listed in Table 2, which reveals that mixed-matrix membranes offer greater void capacity and swell to a higher degree compared with bare PES membrane. This is attributed to the hydrophilic nature of adipate ferroxane and its effects on the mass transfer rate of membrane precipitation during the replacement of solvent (DMAc) and non-solvent (water) in the coagulation bath of phase inversion processes [26].

In the coagulation bath, the higher affinity of adipate ferroxane nanoparticles than that of PES to water caused the penetration velocity of water into the polymer backbone to increase with nanoparticle content during phase inversion. Moreover, the addition of adipate ferroxane can increase DMAc diffusion velocity from the membrane to water [44].

By blending nanoparticles into the casting solution, the interaction between polymer and solvent molecules declined and facilitated the diffusion of solvent molecules from the polymer matrix to the coagulation bath [26]. Additionally, by blending the nanoparticles in to the casting solution of the polymer, the interaction between polymer-chain segments and nanoparticles may disrupt the polymer chain packing, therefore creating greater free volume between the polymer chains and the nanofiller interface than the nascent PES membrane [45]. This effect facilitates water molecule penetration through the membranes and subsequently enhances the flux.

Membrane surface hydrophilicity is another significant factor that can affect the flux and the antifouling ability of a membrane. The sessile drop technique was used for the contact angle measurements, reflecting (determining) characterization of the membrane surface hydrophilicity. Table 2 reports the measured contact angle of nanocomposite membranes. The contact angle decreased with the increase in NPs incorporation in the casting solution. This observation was due to the fact that hydrophilic characteristic of adipate ferroxane increased hydrophilicity of membranes' surface.

The unfilled PES membrane (M_0) showed the highest water contact angle of 68.12° and therefore the lowest hydrophilicity compared with the modified membranes. The addition of 0.2, 0.6 and, 1.0 wt% AFNPs reduced the contact of water angles to 60.33°, 55.04° and 54.73°, respectively, due to the presence of the -OH and -COOH functional groups of the AFNPs.

The reduction in the water contact angles and enhanced hydrophilicity can be attributed to the affinity of adipate ferroxane nanoparticles to water, and therefore their spontaneous migration to the membrane/water interface during the phase inversion process to decrease the interface energy [46,47]. When comparing the top and bottom surface photographs of bare and embedded PES membranes displayed in Fig. 7, the difference between the colors is clearly recognizable.

The color of the membrane's top surface (water exposed side in the phase inversion process) was much darker than the bottom surface (glass side), which indicates the migration of hydrophilic adipate ferroxane to the top-layer surface of the membranes toward water. This migration decorates the functional groups of adipate ferroxane on the membrane's top surface and improves its hydrophilicity. Similar behaviors were also reported by many researchers for different nanofillers during phase inversion [47,48].

Generally, the pure water flux is enhanced with the addition of a suitable amount of nanoparticles in to the casting solution. However, 1.0 wt% content of adipate ferroxane caused a reduction in flux. This could be ascribed to the blocking of pores with high nanoparticle concentrations [49], which was noticed as a reduction in porosity (Table 2) for the prepared membrane. Moreover, the high concentration of adipate ferroxane nanoparticles reduced the pore size and brought about the forming of a pore wall. This can be illustrated by an increase in viscosity of the casting solution, pre-

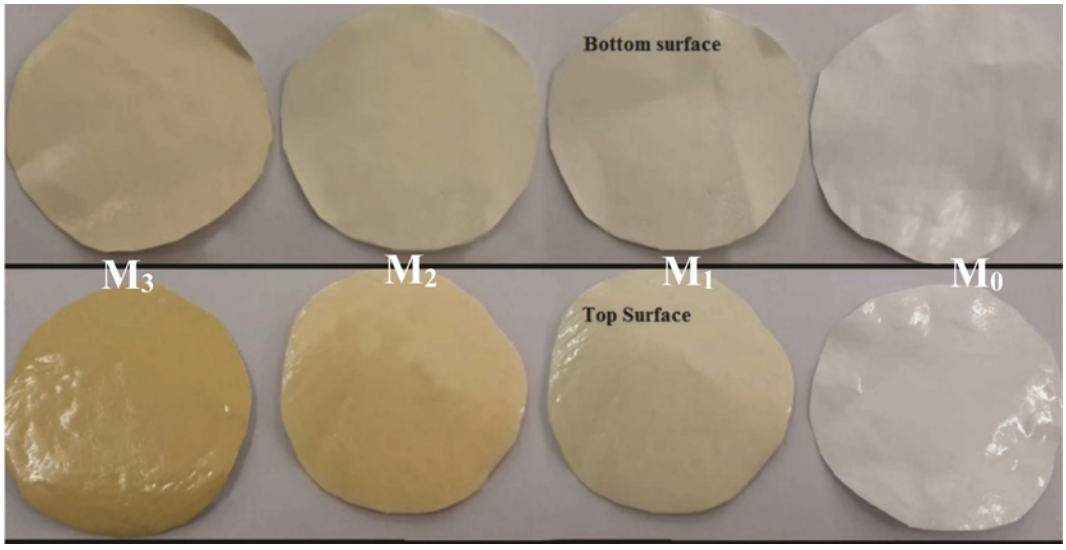

Fig. 7. Digital photograph of top and bottom surface of pristine and embedded PES membranes: (M_0) Unfilled PES, (M_1) 0.2 wt%, (M_2) 0.6 wt%, (M_3) 1 wt%.

venting mixing of the solvent and non-solvent in the coagulation bath. This suppresses the formation of macro-voids, reduces the porosity subsequently, reduces permeation flux [50]. The more than 98% rejection of milk powder proteins by all prepared membranes also indicated that the increase in flux was not related to defects or membrane fracture weak adhesion between the adipate ferroxane nanoparticles and the polymer.

3. Evaluation of Antifouling Properties

To evaluate the antifouling properties of bare and modified PES nanofiltration membranes, cyclic filtration tests with milk powder solution as a good foulant (8,000 mg/L) were performed [45]. The time-dependent flux during the filtration operation is presented in Fig. 8.

In each trend of cyclic filtration, three phases can be seen. The first hour in the curve is referred to as pure water filtration. The second phase is 1-hour foulant solution filtration, and the third phase is a simple membrane cleansing with pure water (about 15 min immersion in distilled water). Then the pure water flux was measured again for another hour. The decline in flux of the membranes can be attributed to foulant (especially proteins) adsorption and/or convective deposition on the membrane surface. The effects of concentration polarization on permeation flux can be effectively reduced by vigorously stirring the membrane in the dead end filtration test. Therefore, the flux decline of the membranes is caused mostly by membrane fouling.

Moreover, because of the irreversible adsorption of some foulant molecules that may be entrapped in the pores or deposited on membrane surfaces, the water flux values do not completely return to the initial value after washing. This phenomenon was quantified by measuring the flux recovery ratio (FRR) that is illustrated in Fig. 9.

This data clearly demonstrates the suitable application of the embedded membranes. The higher FRR means a better antifouling property for the membrane. As shown, the bare PES membrane demonstrated the lowest FRR (30.0%) because of its high hydrophobicity, while this index increased considerably when adipate ferroxane was added to the polymer matrix (more than 90%). In the best case, seen in the NPs 0.6 wt% membrane, the recovery percentage of membrane flux was 96%. The hydrophilicity of the membrane surface was improved by incorporating carboxylate

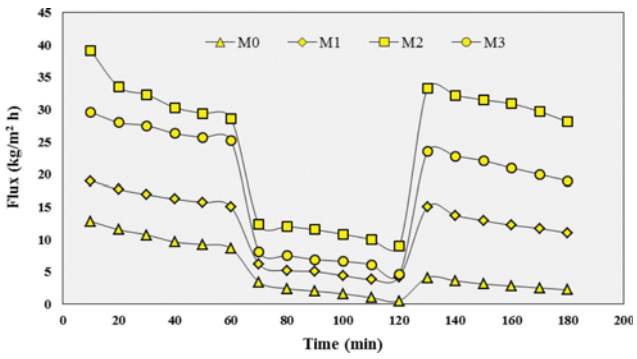

Fig. 8. Time-dependent flux of the prepared membranes.

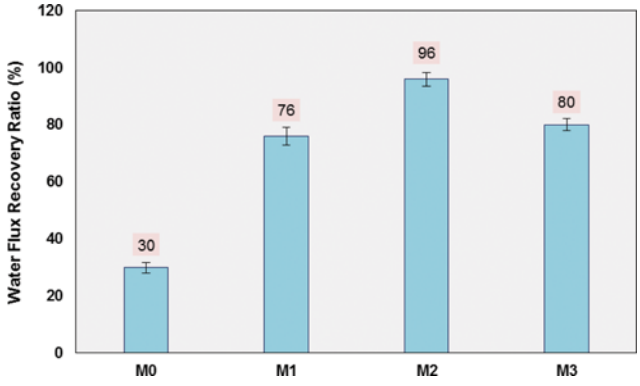

Fig. 9. Water flux recovery ratio of the prepared membranes after Milk powder fouling (average of three replicates was reported).

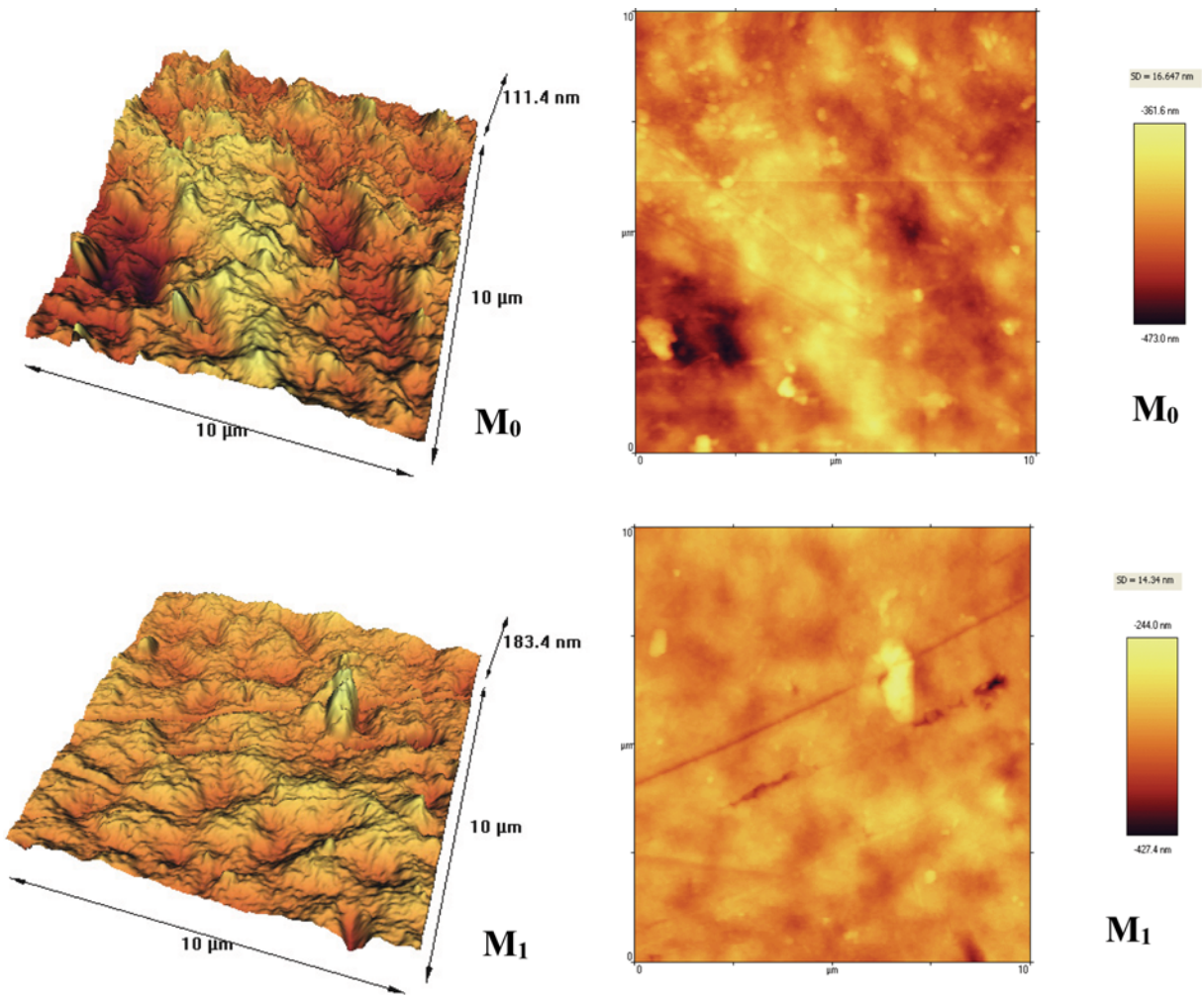

Fig. 10. Surface AFM images of the nanocomposite membranes: (M_0) Unfilled PES, (M_1) 0.2 wt%, (M_2) 0.6 wt%, (M_3) 1 wt%.

functionalized nanoparticles (Table 2) because of the increased surface coverage of hydrophilic groups.

The formation of hydrogen bonds between the stretched hydrophilic functional groups of the membrane surface and water molecules in the surrounding aqueous environment as well as the formation of the hydration layer were induced between foulants and membrane surfaces, which could affect steric exclusion and foulant adsorption [26,51].

AFM topography images provide additional insights into the effect of the nanoparticles on surface roughness and antifouling property of blended membranes. Fig. 10 shows the AFM images of the prepared membranes in this study. The surface of the membranes consists of different peaks (bright areas) and valleys (dark areas).

The surface roughness of polyethersulfone membranes, blended with AFNPs (M_1, M_2, M_3), was obviously smooth in comparison with PES membrane (M_0).

The lower the concentrations of AFNPs, the more regular the arrangements, as a result of low electrostatic interactions, which was consistent with the results obtained in the previous researches [47,52,53]. By embedding high concentrations of AFNPs (1 wt%) into the casting solution and during phase inversion method, the agglomeration of the nanoparticles was increased; consequently, the surface roughness of the prepared membrane was increased.

However, the surface roughness of bare PES membrane was higher than all modified membranes, which is particularly relevant to previous performed experimental data [26,27].

Results showed that the sequence of changes in FRR was consistent with the membrane surface roughness observed through AFM images. The smooth surfaces of the AFNPs/PES (M_1, M_2 and M_3) membranes caused a higher flux recovery related to the bare membrane (M_0). From the reported literature it was discerned that a membrane with less roughness has stronger antifouling abilities, and membrane fouling is enhanced by increasing the membrane surface roughness [10]. Furthermore, the valleys can be clogged by the high tendency of foulants to be absorbed into the valleys of membranes with coarser surfaces [54]. The M_3 membrane had a higher surface roughness than M_2; therefore, it had lower FRR and antifouling properties, although its hydrophilicity was higher.

To investigate the fouling phenomenon in detail, reversible fouling (R_r), irreversible (R_{ir}) fouling and total fouling (R_t), resistance

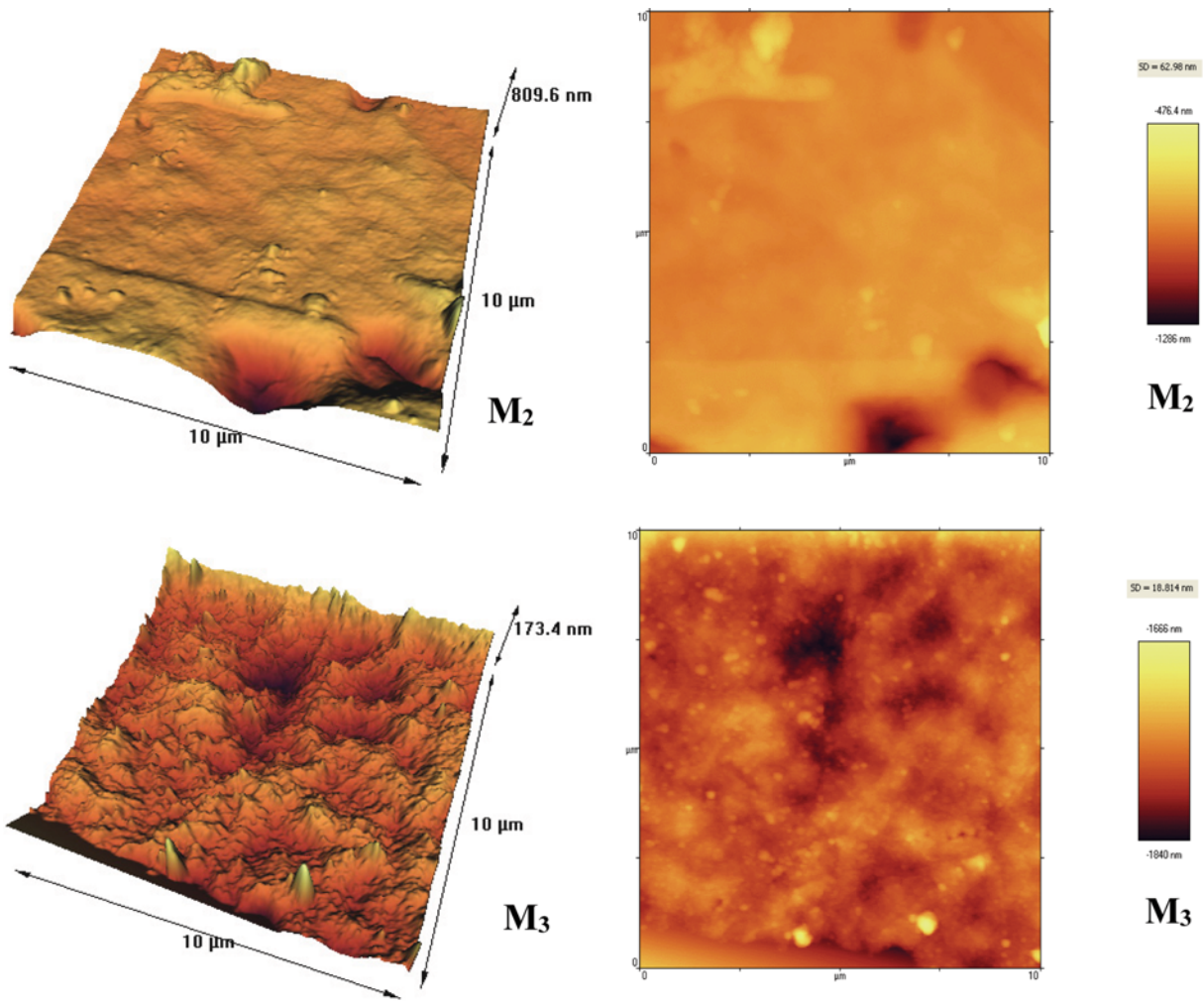

Fig. 10. Continued.

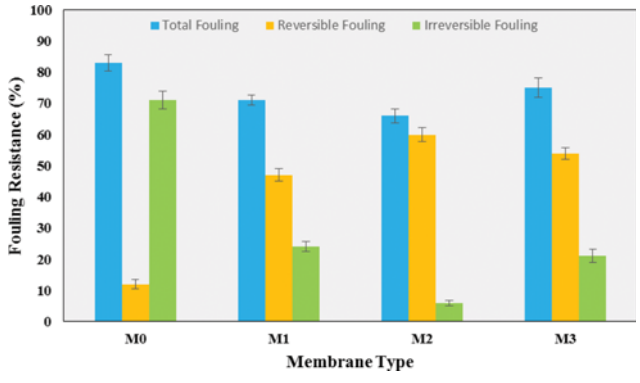

Fig. 11. Fouling resistance ratio of unfilled PES and adipate ferroxane nanoparticles embedded PES membranes.

ratios were calculated and are depicted in Fig. 11.

Results indicated that embedding low amounts of adipate ferroxane (0.2 wt%) in to PES caused irreversible fouling ratios to decrease from 71% to 24%. In contrast, the reversible was enhanced from 12% to 47%. This was caused by the lower surface hydrophilicity and higher surface roughness of the bare PES related to the M_1 membrane, pointing to the better detaching of absorbed foulants through the washing process compared with the embedded membrane surface. Furthermore, adding a high concentration of adipate ferroxane (from 0.6 wt% to 1.0 wt%) to the membrane matrix led to a decrease in reversible fouling from 60% to 54%, which was even higher than that of the unfilled membrane.

Comparing the similar trend of roughness parameters with the sequence changing of the irreversible fouling ratio revealed that surface roughness influenced the alleviation of the membrane irreversible fouling more than the hydrophilicity improvement. Therefore, reduction of surface roughness is the dominant phenomenon in fouling mitigation related to hydrophilicity improvement. This trend was also reported in previous works [15].

4. Rejection Performance

In this work, the nanofiltration performance of bare and adipate ferroxane nanoparticle-embedded membranes was evaluated through dye removal and salt retention capability. For this purpose, first, a solution of direct red 16 at a concentration of 30 mg/L, pH 6, and operating pressure of 4 bar was filtered in a dead-end cell over 90 min. The retention results are shown in Fig. 12.

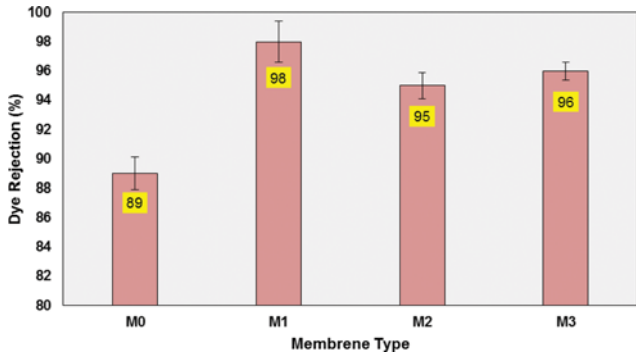

Fig. 12. Dye removal ability of the prepared adipate ferroxane nanoparticle/PES nanofiltration membrane (0.4 MPa, pH 6.0±0.1, 30 mg/L direct red 16, after 90 min filtration).

Fig. 13. The photographs of (right) feed solution, (middle) permeate of M_0 membrane and (left) permeate of M_1 membrane.

The rejection of direct red 16 by the bare PES membrane was 89%, and that was enhanced to about 98.0% for the nanoparticle-embedded membranes. This is a typical behavior of mixed-matrix nanofiltration membranes. A photograph of the feed and permeate solutions is shown in Fig. 13. It represents the better performance of the 0.2 wt% AFNPs/PES membrane in compare with unfilled PES membrane for dye solution treatment.

Generally, two different mechanisms have an important role in the nanofiltration process, Donnan exclusion and steric hindrance, associated with the surface charge and the membrane pore size, respectively [55]. The porosity of the AFNPs/PES membranes is higher than unfilled PES membrane (see Table 2). However, the rejection of AFNPs/PES membranes is higher. This is due to functional groups of adipate ferroxane nanoparticles, which makes negative charge on the membrane surface.

The implied negatively-charged surface of the embedded membranes repels the dye with negative charge that leads to higher rejection; this indicates that Donnan exclusion was more prevailing than steric factors for these nanocomposite mixed-matrix membranes in the separation of dye.

Sorption/adsorption of the dye by adipate ferroxane nanoparticles is one of the other mechanisms for explaining the improvement in dye removal by nanocomposite mixed-matrix membranes.

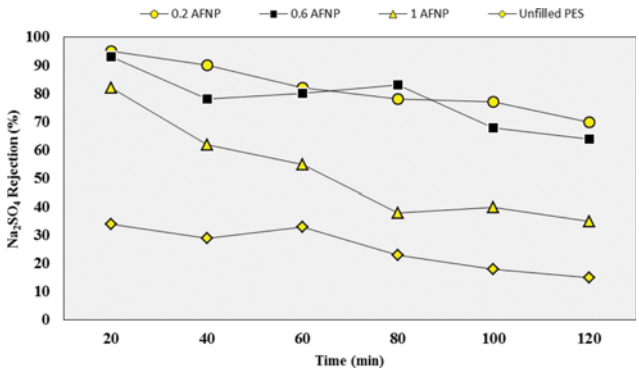

Fig. 14. Na_2SO_4 retention by AFNPs/PES membranes versus time (4 bar, pH 7.0±0.1, 200 ppm salt).

Hydrogen bonding interaction attributed to the presence of the carboxylic, hydroxyl and sulfonic group dissociation of adipate ferroxane nanoparticles and direct red 16 caused adsorption of the dye by membrane surface and membrane inside pore structure. Reduction in dye removal of the 0.6 wt% AFNPs/PES membrane can be attributed to the increasing of membranes porosity and fluxes.

Another typical method to evaluate the separation capability of the mixed-matrix nanofiltration membranes is a rejection test with salt solutions. Salt retention measurements with NaCl, Na_2SO_4 and $MgSO_4$ at the pressure of 4 bar were carried out with the dead-end cell in pH 7. The variation of Na_2SO_4 rejection of prepared mixed-matrix membranes is shown in Fig. 14.

The rejection of Na_2SO_4 was 70, 64, and 35% for 0.2, 0.6, and 1.0 wt% adipate ferroxane/PES membranes, respectively, and 15% for the unfilled PES membrane. Existence of low amount of 0.2 wt% adipate ferroxane nanoparticles initially increased the rejection capability of the membrane. By adding up the concentration of AFNPs in the casting solution, the rejection of Na_2SO_4 was decreased. The salt retention behavior of the 0.2 wt% AFNPs/PES membrane is shown in Fig. 15. From the results, the retention sequence was R (Na_2SO_4)>R ($MgSO_4$)>R (NaCl) that confirmed the lowest retention for a monovalent ion pair and the highest retention for the bivalent anion, whereas presence of the bivalent

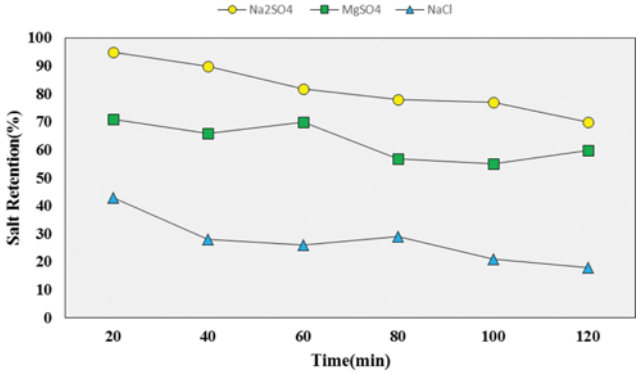

Fig. 15. Salt retention by 0.2 wt% AFNPs/PES membrane (4 bar, pH 7.0±0.1, 200 ppm salt).

cation (Mg^{2+}) reduced the retention of sulfate anion.

The salt retention measurements showed that the behavior of the adipate ferroxane nanoparticles-embedded membranes could be classified as Donnan exclusion mechanism [56,57]. In an aqueous solution, dissociation of surface functional groups gives an electric charge to membranes and causes electrostatic rejection of charged solutes [58]. Three important parameters for the charge exclusion of ions are the ionic strength, the charge of the membrane, and the valence of the ions [57]. The concentration difference of counter-ions, which have the opposite charge and co-ions with the same charge, at the interface between the membrane and an electrolyte solution cause to generate a potential difference. This potential provides an equilibrium between membrane and solution electrochemically, the membrane attracts counter-ions and rejects co-ions [59]. The high retention of Na_2SO_4 (bivalent co-ion, monovalent counter-ion) and the lower retention of NaCl (monovalent co-ion, monovalent counter-ion) agree to Donnan exclusion mechanism.

CONCLUSION

Adipate ferroxane was used as a novel functionalized nanofiller with extra hydroxyl and carboxylic groups on its surface to prepare a mixed-matrix nanofiltration PES membrane through solution casting by the phase inversion method. The results showed that blending adipate ferroxane nanoparticles enhanced membrane flux, surface properties, antifouling and separation characteristics.

The maximum and minimum pure water flux of the embedded membranes are 32.2 kg/m^2h and 16.75 kg/m^2h, that is higher than the bare PES membrane (10.4 kg/m^2h); however, the AFNPs agglomeration at high concentration decreased pure water flux.

The contact angle and porosity measurement demonstrated that adding adipate ferroxane nanoparticles to the casting solution increased hydrophilicity and overall porosity of the embedded membranes which is attributed to the concentrated hydrophilic functional groups on membrane surface that migrated to the top surface during phase inversion in a coagulation bath. Antifouling characteristics of the adipate ferroxane-embedded membranes were improved by the increased hydrophilicity and decrease in membrane surface roughness. The 0.6 wt% AFNPs/PES membrane exhibited the highest FRR (96%) and the lowest surface roughness (according to the AFM images) and irreversible fouling resistance (6%). The SEM images showed that blending adipate ferroxane nanoparticles increased the porosity of both top and sub-layer of the blended membranes.

To investigate the rejection performance, a solution of direct red 16 and salt solutions was filtered, and the results indicated a higher rejection of the embedded membranes compared with that of the bare PES. Also, the rejection behavior of AFNPs/PES membranes indicated that the mechanism of rejection is Donnan exclusion.

REFERENCES

1. B. Van der Bruggen, *J. Appl. Polym. Sci.*, **114**, 630 (2009).
2. Z. Q. Tang, W. Li, J. Zhou, H. Y. Yu, L. Huang, M. G. Yan, J. S. Gu and X. W. Wei, *Sep. Purif. Technol.*, **64**, 332 (2009).
3. T. Barroso, M. Temtem, T. Casimiro and A. Aguiar, *J. Supercrit. Fluids*, **56**, 312 (2011).
4. A. G. Fane, P. Beatson and H. Li, *Water Sci. Technol.*, **41**, 303 (2000).
5. J. Luo, L. Ding, Y. Wan and M. Y. Jaffrin, *Chem. Eng. J.*, **181**, 397 (2012).
6. T. M. Patel and K. Nath, *Desalination*, **317**, 132 (2013).
7. X. Wei, Z. Wang, F. Fan, J. Wang and S. Wang, *Desalination*, **251**, 167 (2010).
8. R. Liikanen, J. Yli-Kuivila and R. Laukkanen, *J. Membr. Sci.*, **195**, 265 (2002).
9. A. Simon, W. E. Price and L. D. Nghiem, *Sep. Purif. Technol.*, **113**, 42 (2013).
10. D. Rana and T. Matsuura, *Chem. Rev.*, **110**, 2448 (2010).
11. R. F. Susanti, Y. S. Han, J. Kim, Y. H. Lee and R. G. Carbonell, *J. Membr. Sci.*, **440**, 88 (2013).
12. C. Ba, D. A. Ladner and J. Economy, *J. Membr. Sci.*, **347**, 250 (2010).
13. C. Wang, R. Feng and F. Yang, *J. Colloid Interface Sci.*, **357**, 273 (2011).
14. Q. Shi, Y. Su, W. Chen, J. Peng, L. Nie, L. Zhang and Z. Jiang, *J. Membr. Sci.*, **366**, 398 (2011).
15. V. Vatanpour, S. S. Madaeni, L. Rajabi, S. Zinadini and A. A. Derakhshan, *J. Membr. Sci.*, **401-402**, 132 (2012).
16. V. Vatanpour, S. S. Madaeni, A. R. Khataee, E. Salehi, S. Zinadini and H. A. Monfared, *Desalination*, **292**, 19 (2012).
17. W. Zou, Y. Huang, J. Luo, J. Liu and C. Zhao, *J. Membr. Sci.*, **358**, 76 (2010).
18. A. Rahimpour and S. S. Madaeni, *J. Membr. Sci.*, **360**, 371 (2010).
19. C. I. Escobar, M. H. Eric, J. G. Christopher and A. D. Francis, *J. Am. Water. Works. Ass.*, **97**, 79 (2005).
20. J. B. Li, J. W. Zhu and M. S. Zheng, *J. Appl. Polym. Sci.*, **103**, 3623 (2007).
21. J.-F. Li, Z.-L. Xu, H. Yang, L.-Y. Yu and M. Liu, *Appl. Surf. Sci.*, **255**, 44725 (2009).
22. J. Kim and B. V. der Bruggen, *Environ. Pollut.*, **158**, 2335 (2010).
23. A. Rahimpour, M. Jahanshahi, B. Rajaeian and M. Rahimnejad, *Desalination*, **278**, 343 (2011).
24. F. Liu, M. R. Moghareh Abed and K. Li, *J. Membr. Sci.*, **366**, 97 (2011).
25. L.-Y. Yu, Z.-L. Xu, H.-M. Shen and H. Yang, *J. Membr. Sci.*, **337**, 257 (2009).
26. S. Zinadini, A. A. Zinatizadeh, M. Rahimi, V. Vatanpour and H. Zangeneh, *J. Membr. Sci.*, **453**, 292 (2014).
27. V. Vatanpour, S. S. Madaeni, R. Moradian, S. Zinadini and B. Astinchap, *J. Membr. Sci.*, **375**, 284 (2011).
28. Z.-Q. Huang, K. Chen, S.-N. Li, X.-T. Yin, Z. Zhang and H.-T. Xu, *J. Membr. Sci.*, **315**, 164 (2008).
29. P. Xu, G. M. Zeng, D. L. Huang, C. L. Feng, S. Hu, M. H. Zhao, C. Lai, Z. Wei, C. Huang, G. X. Xie and Z. F. Liu, *Sci. Total. Environ.*, **424**, 1 (2012).
30. J. Ma, Z. Wang, M. Pan and Y. Guo, *J. Membr. Sci.*, **341**, 214 (2009).
31. C. C. Zhang, X. Li, Y. Yang and C. Wang, *Appl. Phys. A.*, **97**, 281 (2009).
32. N. Ghaemi, S. S. Madaeni, P. Daraei, H. Rajabi, S. Zinadini, A. Alizadeh, R. Heydari, M. Beygzadeh and S. Ghouzivand, *Chem. Eng. J.*, **263**, 101 (2015).

33. P. Daraei, S. S. Madaeni, N. Ghaemi, E. Salehi, M. A. Khadivi, R. Moradian and B. Astinchap, *J. Membr. Sci.*, **415-416**, 250 (2012).
34. P. Sabbatini, F. Rossi, G. Thern, A. Marajofsky and M. de Cortalezzi, *Desalination*, **248**, 184 (2009).
35. P. Sabbatini, F. Yrazu, F. Rossi, G. Thern, A. Marajofsky and M. Fidalgo de Cortalezzi, *Water. Res.*, **44**, 5702 (2010).
36. S. J. Maguire-Boyle, M. V. Liga, Q. Li and A. R. Barron, *Nanoscale*, **4**, 5627 (2012).
37. L. Zhang, S.-R. Chae, S. Lin and M. R. Wiesner, *Environ. Eng. Sci.*, **29**, 124 (2012).
38. M. M. Cortalezzi, J. Rose, G. F. Wells, J. Y. Bottero, A. R. Barron and M. R. Wiesner, *J. Membr. Sci.*, **227**, 207 (2003).
39. S. Rahimi, R. M. Moattari, L. Rajabi, A. A. Derakhshan and M. Keyhani, *J. Ind. Eng. Chem.*, **23**, 33 (2015).
40. J. Saiena, M. Asgari, A. R. Soleymani and N. Taghavinia, *Chem. Eng. J.*, **151**, 295 (2009).
41. N. Daneshvar, A. Aleboyeh and A. R. Khataee, *Chemosphere*, **59**, 761 (2005).
42. E. Bagheripour, A. Moghadassi and S. M. Hosseini, *Korean J. Chem. Eng.*, **33**, 1462 (2016).
43. M. Moochani, A. Moghadassi, S. M. Hosseini, E. Bagheripour and F. Parvizian, *Korean J. Chem. Eng.*, **33**, 2674 (2016).
44. T.-H. Bae and T.-M. Tak, *J. Membr. Sci.*, **249**, 1 (2005).
45. L. Ge, Z. Zhu and V. Rudolph, *Sep. Purif. Technol.*, **78**, 76 (2011).
46. E. Celik, L. Liu and H. Choi, *Water. Res.*, **45**, 5287 (2011).
47. S. Zinadini, A. A. Zinatizadeh, M. Rahimi, V. Vatanpour, H. Zangeneh and M. Beygzadeh, *Desalination*, **349**, 145 (2014).
48. E. Celik, H. Park, H. Choi and H. Choi, *Water Res.*, **45**, 274 (2011).
49. H. Wu, B. Tang and P. Wu, *J. Membr. Sci.*, **362**, 374 (2010).
50. M. J. Han and S. T. Nam, *J. Membr. Sci.*, **202**, 55 (2002).
51. X. Zhao, J. Ma, Z. Wang, G. Wen, J. Jiang, F. Shi and L. Sheng, *Desalination*, **303**, 29 (2012).
52. S. Qiu, L. Wu, X. Pan, L. Zhang, H. Chen and C. Gao, *J. Membr. Sci.*, **342**, 1-2 (2009).
53. H. Zhao, L. Wu, Z. Zhou, L. Zhang and H. Chen, *Phys. Chem. Chem. Phys.*, **15**, 9084 (2013).
54. E. M. Vrijenhoek, S. Hong and M. Elimelech, *J. Membr. Sci.*, **188**, 115 (2001).
55. S. K. Maurya, K. Parashuram, P. S. Singh, P. Ray, AVR. Reddy, *Desalination*, **304**, 11 (2012).
56. S. Sarkar, A. K. Sengupta and P. Prakash, *Environ. Sci. Technol.*, **44**, 1161 (2010).
57. M. Nilsson, G. Trägårdh and K. Östergren, *J. Membr. Sci.*, **312**, 97 (2008).
58. M. Elimelech, W. H. Chen and J. J. Waypa, *Desalination*, **95**, 269 (1994).
59. J. M. M. Peeters, J. P. Boom, M. H. V. Mulder and H. Strathmann, *J. Membr. Sci.*, **145**, 199 (1998).